# SPATIAL CHARACTERISTICS OF THE MIMO WIRELESS CHANNEL: EXPERIMENTAL DATA ACQUISITION AND ANALYSIS

*Jon W. Wallace and Michael A. Jensen*

Brigham Young University
Electrical and Computer Engineering Dept.
459 CB, Provo, UT 84602
wallacej@et.byu.edu, jensen@ee.byu.edu

## ABSTRACT

Detailed performance assessment of space-time coding algorithms in realistic channels is critically dependent upon accurate knowledge of the wireless channel spatial characteristics. This paper presents an experimental measurement platform capable of providing the channel transfer matrix for indoor and outdoor wireless communications scenarios. The system allows direct measurement of key multiple input multiple output parameters for 16 transmit and 16 receive antennas. The basic hardware blocks are outlined, and the data post-processing algorithms are presented. Representative data showing channel capacity and spatial correlation for several indoor sites are provided.

## 1. INTRODUCTION

The increasing demand for capacity in wireless systems has motivated considerable research aimed at achieving higher throughput on a given bandwidth. One important finding of this activity is the recent demonstration that for an environment sufficiently rich in multipath components, the wireless channel capacity can be increased using multiple antennas on both transmit and receive sides of the link [1]–[4]. Algorithms that achieve this increased capacity actually *exploit* the multipath structure by cleverly coding the data in both time and space. Therefore, in order to assess the performance of systems that implement these algorithms, we must gain an improved understanding of the complex spatial behavior of wireless multiple input multiple output (MIMO) channels [5].

Past methods for characterizing multipath MIMO channels include approximate statistical analyses and costly ray tracing procedures. These solutions tend to be of limited usefulness as they cannot accommodate an adequately detailed representation of the channel. In this work, we report the development of an experimental platform designed to measure the transfer matrix for indoor and outdoor MIMO channels. The key aspects of the hardware system and the data processing are presented. Representative data obtained with the instrument in several indoor environments are also provided. These results reveal the large increase in capacity that can be achieved using MIMO architectures coupled with space-time coding implementations.

This work was supported by the National Science Foundation under Wireless Initiative Grant CCR 99-79452.

## 2. MEASUREMENT SYSTEM

The goal of this effort is to directly measure the wireless MIMO channel transfer matrix $\mathbf{H}$, where the element $H_{mn}(\omega)$ represents the frequency dependent transfer function between the $n^{th}$ transmitter and $m^{th}$ receiver antennas. The experimental platform, depicted in Figure 1, uses a custom MIMO communications system operating between 0.8 and 6 GHz. The transmitter uses a digital pattern generator (DPG) to create $N$ unique binary ($\pm 1$) codes. These codes are fed into a custom RF chassis where they are mixed with a local oscillator (LO) to produce $N$ distinct co-channel binary phase shift keyed (BPSK) signals. The resulting signals are amplified to 0.5 W and fed into one of the $N$ transmit antennas. The receiver uses a custom RF chassis to amplify and downconvert the signals from each of the $M$ antennas. The resulting $M$ intermediate frequency (IF) signals are low-pass filtered, amplified, and sampled using a 16-channel 1.25 Msample/s A/D card for storage on the PC.

## 3. DATA PROCESSING

The raw data collected using the measurement platform is processed to obtain estimates of the time-variant channel matrix. The technique consists of 3 basic steps: (1) code search, (2) carrier recovery, and (3) channel estimation.

### 3.1. Code Search

The first step in the data post-processing is to determine the alignment of the modulating codes. As shown in Figure 2, the method begins by correlating the signal from one of the $M$ receive antennas with a baseband representation of one of the transmit codes. An FFT of this result produces a peak at the IF when the known code and the code in the receive signal are aligned. The process uses adaptive step size selection and shortened codes to expedite the search process. Additionally, the procedure searches over every combination of receive channel and codeword, ensuring accurate code synchronization even in situations where a fraction of the signals undergo severe attenuation.

### 3.2. Carrier Recovery

The IF estimated during the code search process is refined using a subplex optimization loop that maximizes the magnitude of the Discrete Time Fourier Transform (DTFT) of the despread signal (known aligned code multiplied by the receive signal). Following

0-7803-7041-4/01/$10.00 ©2001 IEEE

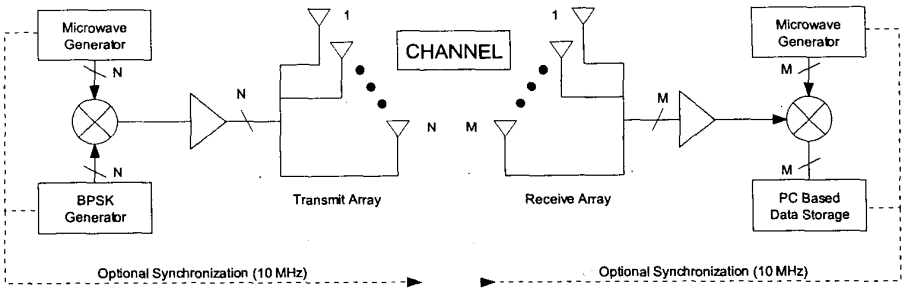


**Fig. 1**. High level system diagram of the narrowband wireless MIMO measurement system

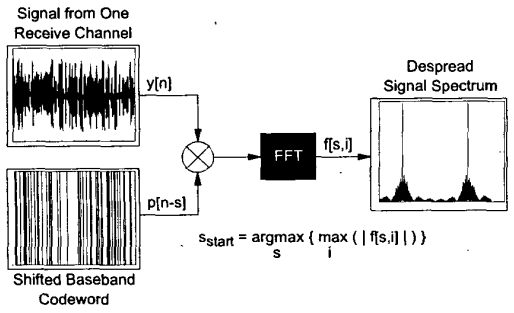


**Fig. 2**. Basic method for finding codeword start sample when exact carrier frequency is unknown.

frequency estimation, the phase variation is recovered by moving a window along the despread signal and correlating this waveform against a complex sinusoid at the estimated IF frequency, as shown in Figure 3. The phase of this result represents the phase at the center of the recovery window. An averaging window is then used to smooth this phase estimate.

### 3.3. Channel Estimation

The IF signal on the $m^{th}$ receive channel is composed of $N$ BPSK codes, with each code possessing an amplitude $A_{mn}$ and phase $\phi_{mn}$. If $p_n[k]$ represents the $k^{th}$ sample of the $n^{th}$ code, the discrete received signal is given as

$$y_m[k] = \sum_{n=0}^{N-1} A_{mn}\, p_n[k]\, \cos(\Omega_1 k + \phi_k + \phi_{mn}) \qquad (1)$$

where $\Omega_1$ is the discrete carrier frequency and $\phi_k$ is the randomly varying carrier phase. Note that for simplicity in deriving the inverse relationship, additive noise has been ignored.

To construct channel matrices, we must infer the channel parameters $A_{mn}$ and $\phi_{mn}$ from the received sequence $y_m[k]$. To obtain a maximum likelihood estimate of these values, we multiply $y_m[k]$ by $p_i[k]$ and the complex signal $c[k] = e^{-j(\Omega_1 k + \phi_k)}$ and subsequently average over $K = (k_2 - k_1 + 1)$ samples to produce

$$R_{mi} = \frac{1}{2K} \sum_{k=k_1}^{k_2} \sum_{n=0}^{N-1} \left[ \widetilde{A}_{mn} + \widetilde{A}^*_{mn} e^{-j2(\Omega_1 k + \phi_k)} \right] p_{ni}[k] \quad (2)$$

where $p_{ni}[k] = p_n[k]p_i[k]$ and $\widetilde{A}_{mn} = A_{mn}e^{j\phi_{mn}}$. Dividing the equation into real and imaginary parts allows the formulation of a block matrix equation that can be solved for the elements $\widetilde{A}_{mn} = H_{mn}$.

## 4. REPRESENTATIVE RESULTS

A variety of measurements have been taken with the experimental platform discussed. In the data shown, a calibration procedure has been applied to remove magnitude and phase errors produced by differences across channels within the system. Additionally, to allow comparison of results obtained from different locations, the measured **H** matrices are normalized such that the average single input single output (SISO) signal-to-noise ratio (SNR) is 20 dB. The carrier frequency is 2.45 GHz with a BPSK code rate of 12.5 kb/s. 1000-bit pseudorandom binary sequences are used, allowing one channel estimate every 0.08 s.

The following table lists the transmit and receive locations, antenna type, and number of 10-second data records considered for this study. Rooms 484 and 400 are centrally-located laboratories, separated by a hallway, within the BYU engineering building. The linear antenna arrays used were 4 single polarization patches with $\lambda/2$ spacing (4SP), 2 dual polarization (V/H) patches with $\lambda/2$ spacing (2DP), and 10 monopole antennas with $\lambda/4$ spacing (10SP).

| Name | Xmit Loc | Recv Loc | Ant | Records |
|---|---|---|---|---|
| 4×4(a) | RM484 | 5 Rooms | 4SP | 233 |
| 4×4(b) | Hall | RM400 | 2DP | 165 |
| 10×10(a) | Hall | RM400 | 10SP | 474 |
| 10×10(b) | RM484 | RM400 | 10SP | 274 |
| 10×10(c) | RM484 | RM400 | 10SP | 120 |

### 4.1. Channel Matrix Element Statistics

Empirical probability density functions (PDFs) for the channel matrix element magnitude and phase were computed by taking histograms assuming each combination of time sample, transmit antenna, and receive antenna represent a single observation. Figures 4 and 5 show the PDFs for element magnitude and phase for sets 4×4(a) and 10×10(a) respectively compared with the Rayleigh distribution with parameter $\sigma^2 = 0.5$ (magnitude) and the uniform distribution on $[-\pi, \pi]$ (phase). The agreement between the analytical and empirical PDFs is excellent. The improved fit for 10×10 data arises from more records and antennas available for averaging.

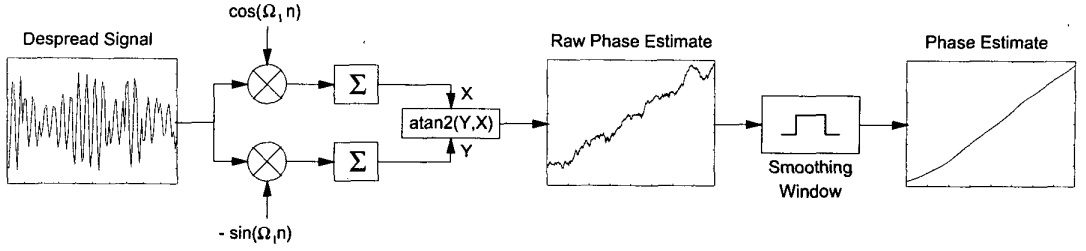


**Fig. 3**. Carrier phase recovery method

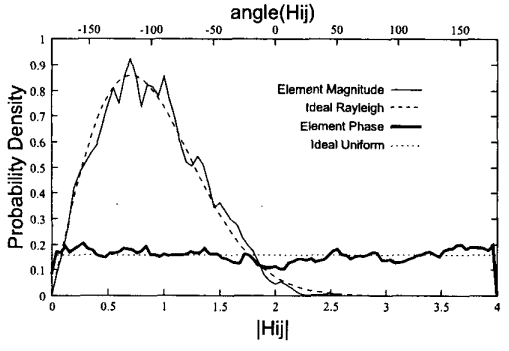


**Fig. 4**. Empirical PDFs for magnitude and phase of the 4×4 **H** matrix elements, compared with Rayleigh and uniform PDFs, respectively.

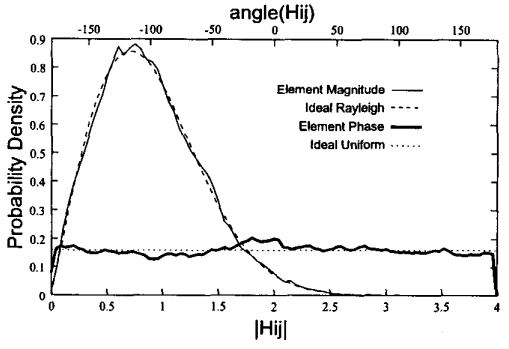


**Fig. 5**. Empirical PDFs for the magnitude and phase of the 10×10 **H** matrix elements.

### 4.2. Channel Correlation

The indoor channel is subject to temporal drift due to such effects as occupant motion and door movement. To assess the time scales of such effects, a temporal correlation coefficient for the **H** matrix elements was computed using all combinations of transmit and receive antennas and starting time sample. Figure 6 plots the magnitude of the temporal correlation coefficient over a period of 5 seconds for each of the data sets considered. The temporal correlation seems to exhibit an exponential decay to a "resting" correlation value. This is reasonable since on short time scales the main disturbances are temporary, causing the channel to oscillate about a constant value. It is also noteworthy that the 10×10(a) and 4×4(a) data sets were taken during periods of low activity, explaining the high correlation observed.

The channel spatial correlation is a physical mechanism that directly impacts the channel capacity. In this study, we assume that the spatial correlation is a separable function in transmit and receive antenna. Receive correlation is found by computing the correlation coefficient of signals on receive antennas separated by a given spacing, over all probe times, locations, and transmit antennas. Transmit correlation is found similarly, by exchanging roles of transmit and receive. Figure 7 shows the transmit and receive correlations compared with Jakes' model [6].

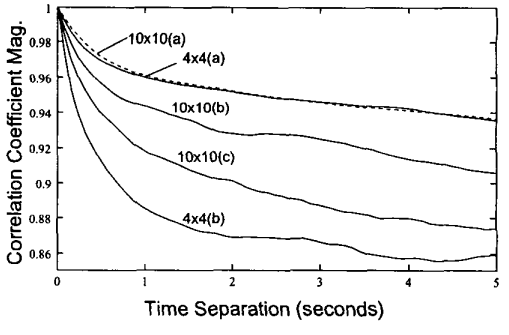


**Fig. 6**. Temporal correlation coefficient over a 5 second interval for all data sets.

### 4.3. Capacity

Channel capacity is computed directly from the measured **H** matrices according to the water-filling solution [4]. Using data set 4×4(b), we examine the capacity for 2×2 matrices using: 1) 2 elements with the same polarization separated by λ/2 (SP), 2) 1 dual-polarization element (DP), 3) 2 elements with orthogonal polarizations and separated by λ/2 (DPS). For comparison, capacity for matrices with iid complex Gaussian-distributed elements (zero mean, unity variance) were also computed with a full-matrix (IID) as well as a diagonal one (DIAG: to approximate the case of zero coupling between orthogonal polarizations). The capacity complementary cumulative distribution functions (CCDF) for this study are shown in Figure 8. As can be seen, polarization diversity produces superior results to spatial diversity due to the low correlation between orthogonally polarized signals.

Figure 9 shows a histogram of capacity across all probing

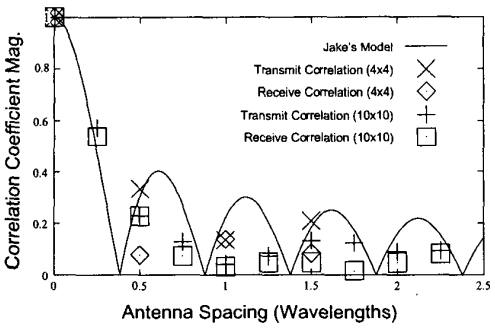


**Fig. 7.** Magnitude of the shift-invariant spatial correlation coefficients at transmit and receive compared with Jakes' model.

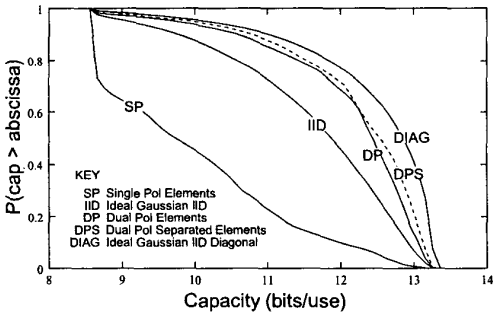


**Fig. 8.** CCDFs for 2×2 channels employing different types of polarization/spatial separation.

times and locations using sets 4×4(a) and 10×10(a)-(c). As can be seen, use of 10 elements significantly increases the available capacity. Using the data of set 10×10(a), we have also investigated the capacity per antenna for 2, 4, and 10 transmit and receive antennas. For consistency, each array has the same total length (2.25 $\lambda$). Figure 10 shows the capacity CCDFs per number of antennas. The curves labeled "Gaussian" represent Monte Carlo simulations for iid complex Gaussian matrix elements. As can be seen, as the number of elements increases, the capacity per channel decreases due to higher correlation between adjacent elements.

## 5. CONCLUSION

Wireless communication systems employing multiple transmit and receive antennas have potentially greater capacity than their single antenna counterparts on the same bandwidth. Understanding the gains that are possible with such systems requires detailed knowledge of the MIMO channel transfer matrix. This paper has presented a system capable of measuring wireless MIMO channel response over the 0.8 to 6 GHz frequency range with up to 16 transmitters and receivers. Data collected by this platform have illustrated the spatial as well as temporal characteristics of the MIMO channel. This data will aid in the assessment of analytical and numerical channel models as well as the formulation of new models which capture the complex spatial behavior of indoor and outdoor multipath environments.

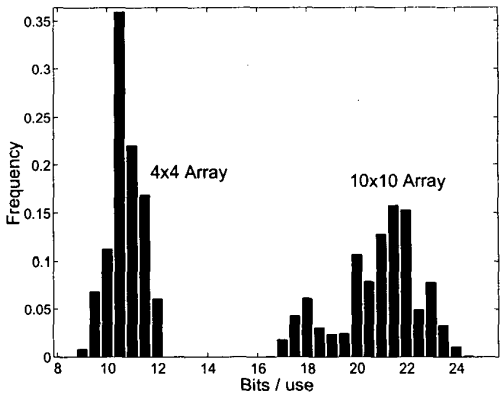


**Fig. 9.** Histogram of capacity over all times and locations.

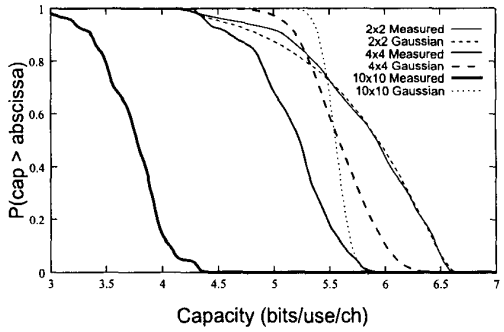


**Fig. 10.** Capacity CCDFs per number of antennas for transmit/receive arrays of increasing number of elements. The array length is 2.25 $\lambda$ for all cases.

## 6. REFERENCES


[1] G. J. Foschini and M. J. Gans, "On limits of wireless communications in a fading environment when using multiple antennas", *Wireless Personal Communications*, vol. 6, no. 3, pp. 311–335, March 1998.

[2] V. Tarokh, N Seshadri, and A. R. Calderbank, "Space-time codes for high data rate wireless communication: Performance criterion and code construction", *IEEE Trans. Information Theory*, vol. 44, no. 2, pp. 744–65, March 1998.

[3] G. Golden, C Foschini, R Valenzuela, and P. Wolniansky, "Detection algorithm and initial laboratory results using V - BLAST space-time communication architecture", *Electronic Letters*, vol. 35, no. 1, pp. 14–15, Jan. 1999.

[4] Gregory G. Rayleigh and John. M. Cioffi, "Spatio-temporal coding for wireless communication", *IEEE Transactions on Communications*, vol. 46, no. 3, pp. 357–366, March 1998.

[5] Q. Spencer, B. Jeffs, M. Jensen, and A. Swindlehurst, "Modeling the statistical time and angle of arrival characteristics of an indoor multipath channel", *IEEE J. Selected Areas Commun.*, vol. 18, no. 3, pp. 347–360, Mar. 2000.

[6] W. C. Jakes, *Microwave Mobile Communications*, IEEE Press, 1993.